Spontaneous Symmetry Breaking of a Hinged Flapping Filament Generates Lift

Shervin Bagheri[1,3], Andrea Mazzino[1,2] and Alessandro Bottaro[1]
[1] *DICCA, University of Genova, Via Montallegro 1, 16145 Genova, Italy*
[2] *INFN and CINFAI Consortium, Genova Section, Via Dodecaneso 33, 16146 Genova, Italy*
[3] *Linné Flow Centre, KTH Mechanics, 10044 Stockholm, Sweden*
(Dated: August 10, 2012)

Elastic filamentous structures found on swimming and flying organisms are versatile in function, rendering their precise contribution to locomotion difficult to assess. We show in this Letter that a single passive filament hinged on the rear of a bluff body placed in a stream can generate a net lift force without increasing the mean drag force on the body. This is a consequence of spontaneous symmetry breaking in the filament's flapping dynamics. The phenomenon is related to a resonance between the frequency associated to the von-Kárman vortex street developing behind the bluff body and the natural frequency of the free bending vibrations of the filament.

PACS numbers: 46.40.Jj, 47.63.Gd, 47.63.-b, 87.85.gf, 83.10.-y

Intriguing and unexpected properties of the physical universe can be explained and understood in terms of spontaneously broken symmetry [1]. In fluid dynamics, examples of symmetry breaking are known since Jacobi's famous 1834 discovery that a rotating fluid mass could have equilibrium configurations lacking rotational symmetry [2]. More recently, symmetry-breaking of fluid-structure interaction problems have come to play an important role for our understanding of animal locomotion. For example, it has been found that the periodic vertical movement of a symmetric body, which is free to move in the horizontal direction, can spontaneously generate locomotion due to symmetry breaking [3, 4]. Another example is the symmetry-breaking bifurcation of flagella due to a buckling instability, which has a significant impact on the waveform and swimming trajectory of spermatozoa [5].

Our aim here is to provide evidence and physical support for the emergence of symmetry breaking for a simple, even if non-trivial, fluid-structure interaction system. It consists of an elastic filament free to flap in the wake of a two-dimensional (2D) circular cylinder. The filament is anchored to the cylinder and the unperturbed upstream fluid flows parallel to the filament axis. A sketch of the system is shown in Fig. 1. This particular 2D configuration can be experimentally realized using soap-film flows [6, 7]. The following important features characterize all numerical experiments we have performed. When placed in an unperturbed stream, the cylinder alone does not show any symmetry breaking; the flow behind it consists of the celebrated von Kárman street of alternating vortices. Note that the up-down symmetry is not broken and, after half a period, the upper eddies are mirror images of the lower ones. The same up-down symmetry is observed for the filament alone when it undergoes a regular flapping motion [7–9]. When we let the two symmetry-preserving systems interact a surprising feature arises: after a transient we observe a clear symmetry breaking (see Fig. 2), with the filament oscillating in either the upper or the lower part of the cylinder wake. The filament length plays the role of a bifurcation parameter. As we will see, symmetry breaking is associated to a net generation of lift and torque. Consequently, if the system is allowed to move freely, it will experience self-propulsion in the y-direction and rotation around the cylinder axis. Describing and finding possible explanations for the above scenario is the main concern of the present Letter.

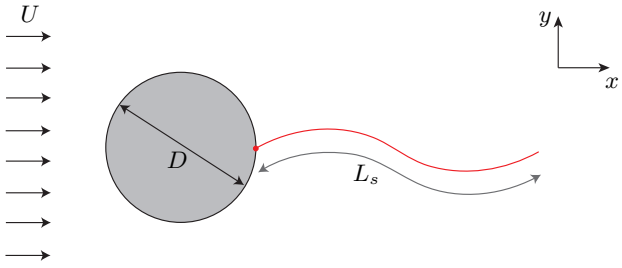

FIG. 1: The simply supported elastic filament anchored to a rigid cylinder subject to a uniform streamwise flow. The initial configuration is symmetric with respect to the normal coordinate y, which is centered on the cylinder.

We consider a two-dimensional inextensible elastic filament of length L_s, mass per unit length ρ_s and flexural rigidity B – as shown in Fig. 1 – attached to the rear of a rigid circular cylinder of diameter D. The filament is surrounded by a viscous incompressible fluid of density ρ_f, kinematic viscosity ν and free stream velocity U. Scaling space and time with D and D/U respectively, four dimensionless parameters arise,

$$Re = \frac{UD}{\nu}, \quad R_1 = \frac{\rho_s}{\rho_f D}, \quad R_2 = \frac{B}{\rho_f U^2 D^3}, \quad L = \frac{L_s}{D},$$

which are the Reynolds number, the mass, the rigidity and the length ratios.

The motion of the fluid and solid is governed by the mass and momentum conservation equations, written in

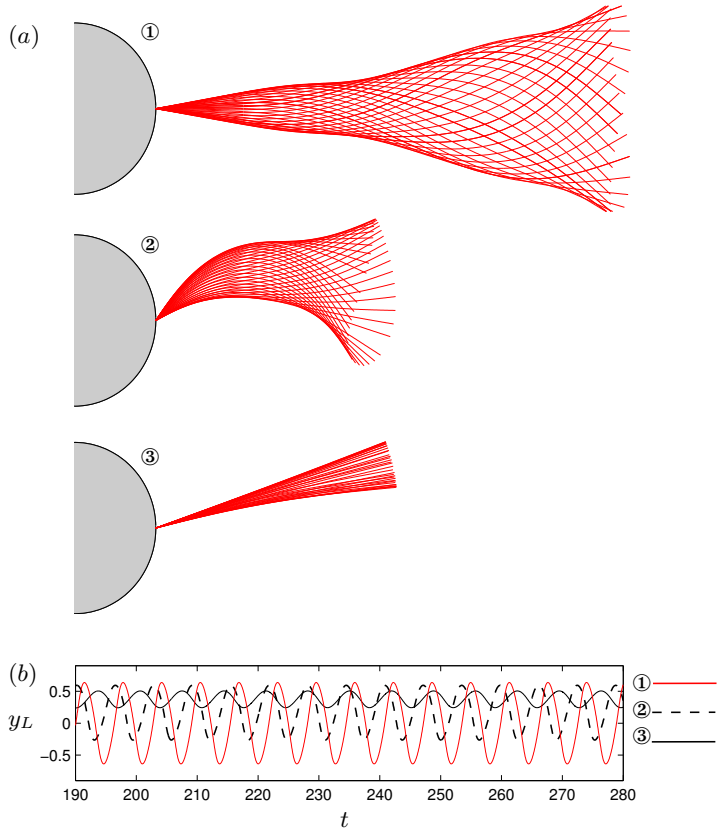

FIG. 2: Red lines in (a) depict the filament position at different times. The symmetric flapping filament ($L = 3, R_2 = 0.005$) is marked with label ①, whereas asymmetric flapping filaments, corresponding to a flexible ($L = 1.5, R_2 = 0.005$) or rigid ($L = 1.5, R_2 = 0.1$) configuration, are marked with labels ② and ③, respectively. For all cases, the other parameters are fixed at $Re = 100$ and $R_1 = 0.1$. In (b), the transverse component of the filament tail position y_L is shown as function of time.

immersed boundary form [10–12],

$$\begin{aligned} \mathbf{u}_t + \mathbf{u}\cdot\nabla\mathbf{u} &= -\nabla p + Re^{-1}\nabla^2\mathbf{u} + \boldsymbol{\lambda} + \mathbf{f}, \\ \nabla\cdot\mathbf{u} &= 0, \\ R_1\mathbf{X}_{tt} &= \partial_s(T\hat{\boldsymbol{\tau}}) - R_2\partial_{ss}(C\hat{\boldsymbol{n}}) + \mathbf{F}. \end{aligned} \tag{1}$$

In the first equation, $\mathbf{u}(\mathbf{x},t)$, $p(\mathbf{x},t)$ and $\boldsymbol{\lambda}(\mathbf{x},t)$ are, respectively, the fluid velocity and Lagrange multipliers to enforce incompressibility of the flow and no-slip condition at cylinder boundary points. The last equation governs the dynamics of the filament position $\mathbf{X}(s,t)$ with a simply supported condition at $s = 0$ and free-end condition at $s = L$. Here, T is the tension, which enforces inextensibility, C is the filament curvature and $\hat{\boldsymbol{\tau}}$ and $\hat{\boldsymbol{n}}$ are unit vectors pointing in the tangential and normal direction of the filament, respectively. The fluid and the filament are coupled at their interface by the no-slip condition $\mathbf{X}_t = \mathbf{U}(\mathbf{X}(s,t),t)$, with $\mathbf{U}(\mathbf{X}(s,t),t) = \int \mathbf{u}(\mathbf{x},t)\delta(\mathbf{x}-\mathbf{X}(s,t))\,d\mathbf{x}$ the Lagrangian filament velocity and $\mathbf{f}(\mathbf{x},t) = \int_s \mathbf{F}(s,t)\delta(\mathbf{x}-\mathbf{X}(s,t))\,ds$, with $\mathbf{f}(\mathbf{x},t)$ the Eulerian force density and $\mathbf{F}(s,t)$ the Lagrangian force density.

The flow past a circular cylinder (without the filament) becomes unstable at $Re \approx 47$ via a Hopf bifurcation, resulting in the emergence of the von Kárman vortex street. The sustained vortex shedding is periodic up to approximately $Re \approx 180$, before the limit cycle becomes unstable to three-dimensional disturbances. Next, let us consider the flexible filament alone, clamped at one end and free at the other in a uniform flow field. If it is sufficiently long or the imposed uniform flow sufficiently strong ($L_s U/\nu \gtrsim 10^3$), its motion is steady for low mass ratios R_1, periodic for intermediate R_1 and finally chaotic for large R_1 [13]. The bending rigidity R_2 has a stabilizing effect on the structure, but for filaments with high bending stiffness R_2, an additional destabilizing effect becomes significant, due to the upstream influence – through modification of pressure – of the vortices shed from the trailing edge [14].

We have numerically solved the governing equations for the flow past the cylinder in the presence of the filament [26]. Fig. 2(a) shows the filament position at different times in the presence of a long filament (label ①), a short filament of small rigidity (label ②) and a short filament of high rigidity (label ③). For $L = 3$ sinuous waves propagate along the filament and amplify as they approach the free end. In the cases of $L = 1.5$ the filament flaps – depending on the initial perturbation – either above or below the $y = 0$ axis. Both the symmetric and asymmetric motions shown in Fig. 2(a) are periodic (see Fig. 2(b)) and synchronized with the von Kárman vortex street. The observed asymmetry develops spontaneously, resulting in a significant net lift force, a reduced mean drag, and the creation of torque on the composite body compared to the cylinder without the filament (see table I).

The equation describing the lateral motion $(Y(s,t))$ of the unforced inextensible filament is $R_1 Y_{tt} + R_2 Y_{ssss} = 0$. The corresponding eigenfrequency is $f_s = [R_2/(R_1 L^4)]^{1/2}$ and constitutes the characteristic time scale associated with the free vibrations of the elastic filament. On the other hand, the characteristic, dimensionless frequency of the flow behind a cylinder at $Re = 100$ is $f_c = fD/U = 0.164$, where f is the vortex shedding frequency. In order to have efficient coupling between the filament's elastic degree of freedom and vortex structures shed by the cylinder, it is expected that the relationship $f_s \sim f_c$ holds. For $f_s \ll f_c$ the filament's elastic response to strain is strongly inhibited because of its slow reaction time. The flow does not feel the filament's elastic degree of freedom with the result that the flow symmetries – prevalent in the absence of filament – are restored. In the opposite limit, $f_s \gg f_c$, the filament instantaneously reacts to strain thus affecting flow properties and its original symmetries. We can formulate the resonance by the condition, $L_r \sim [R_2/(R_1 f_c^2)]^{1/4}$.

The total energy of the filament reads

$$E(t) = \frac{1}{2}\int_0^L R_1|\mathbf{X}_t|^2 + R_2\,|\mathbf{X}_{ss}|^2\;\,ds \qquad (2)$$

where we have disregarded the term due to tensile force, since its contribution is orders of magnitude smaller than the bending term. Since the filament flapping is synchronized with the vortex shedding, D/U is the natural time scale of the filament. However, it is appropriate to consider the non-dimensional filament energy in terms of density ρ_s and length L_s of the filament, instead of ρ_f and D. This results in the following scaling of the total energy $\tilde{E} = E/(R_1 L^3)$. In Fig. 3(a) the mean value of $\tilde{E}$ shows a distinct peak in the response of the flexible and rigid filaments for $L \approx 1.25$ and $L \approx 2.25$, respectively. These values are in good agreement with $L_r = 1.2$ and $L_r = 2.6$ predicted from the resonance condition.

The actual critical values for symmetry-breaking, L_c are in qualitative agreement with the values inferred from the resonance condition L_r. In Fig. 3(b), we show the emergence of a sustained asymmetric flapping state at a well-defined threshold, which takes the value $L_c = 1.5$ and $L_c = 2.1$, for the flexible and stiff filaments, respectively. At this critical condition lift and drag coefficients display a sharp discontinuity. The criterion for asymmetric behavior can be based on a non-zero mean value of the angle Θ formed by the straight line connecting the filament anchor point to its tail position with the x-axis. Note that the angle Θ in Fig. 3(b) does not approach zero for small L, the fingerprint of a possible singularity for $L \to 0$.

The number of filament's bending modes excited increases with its flexibility, resulting in a dynamically more complex fluid-structure interaction. For the flexible structure this results in a third regime for intermediate values of the length ratio ($1.6 < L < 2.5$) where the filament behavior is quasi-periodic or even chaotic. In this regime, each shed von Kárman vortex slightly deflects the filament from its asymmetric position towards the opposite side. As a consequence, travel back and forth between the upper and lower regions on a slow time scale as they undergo synchronized undulations with the vortex street on a fast time scale, resulting in a quasi-periodic motion. We do not exclude the possibility for further asymmetric states in the chaotic regime.

In the region of reversed flow behind the cylinder (for $Re = 100$ this extends up to $x = 1.9D$ for the time-averaged flow) the filament is interchangeably compressed and stretched; outside this region, the filament is exposed to stretching. This induces a nonuniform tension on the filament in order to oppose the stretching and compressive viscous stress. The filament also has a restoring force due to its bending rigidity; if it is too flexible ($R_2 \lesssim 10^{-4}$), it is unable to resist the pressure drag [15] exerted by the back flow and collapses towards the cylinder. Note that flexibility is not necessary for

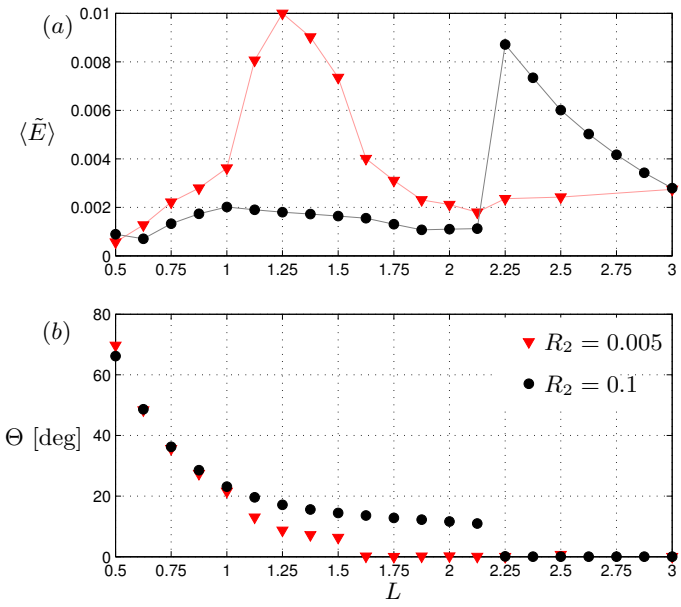

FIG. 3: (a) Mean value of the total filament energy $\langle\tilde{E}\rangle$ as a function of the filament length, demonstrating the resonance behavior between hydrodynamic and elastic degrees of freedom. (b) Average value Θ as function of L. The crossover from non-zero to zero values of Θ is the fingerprint of the bifurcation from symmetric to asymmetric flapping motion. Parameters are $Re = 100$, $R_1 = 0.1$.

symmetry breaking; therefore – and in contrast to observations made for Stokes flows [5] or Non-Newtonian fluids [16] – the trapping of the filament in either the lower or upper half-plane is not due to the buckling instability of a flexible filament.

In order to highlight how the filament interacts with the unsteady vortical structures in the recirculation region, we compute the maximum value of the finite-time Lyapunov exponent (FTLE). Contours of FTLE correspond to precise vortex boundaries and reveal Lagrangian coherent structures [17, 18] in a similar fashion as visualization techniques based on injection of "tracers", such as dye or smoke. Fig. 4 shows maximum values of FTLE of instantaneous flow fields. The near field of the vortex street is nearly left unaltered in the presence of the long filament reported in Fig. 4(a), in contrast to the short filaments shown in Figs. 4(b) and 4(c). The snapshots in Figs. 4(b) and 4(c) correspond to shortly after the beginning of the upward movement of the filaments. At this instant there is a significant compressive fluid force; in order to resist compression the short filaments induce vorticity with negative (clockwise) circulation. For the flexible filament (Fig. 4(b)), the emergence of a co-rotating vortex pair separated by the flexible filament is clearly visible. The more rigid filament (Fig. 4(c)) releases a vortex from its trailing edge with the same rotation as the upper cylinder vortex [27]. The filament-induced vorticity in the wake breaks the symmetry by modifying the

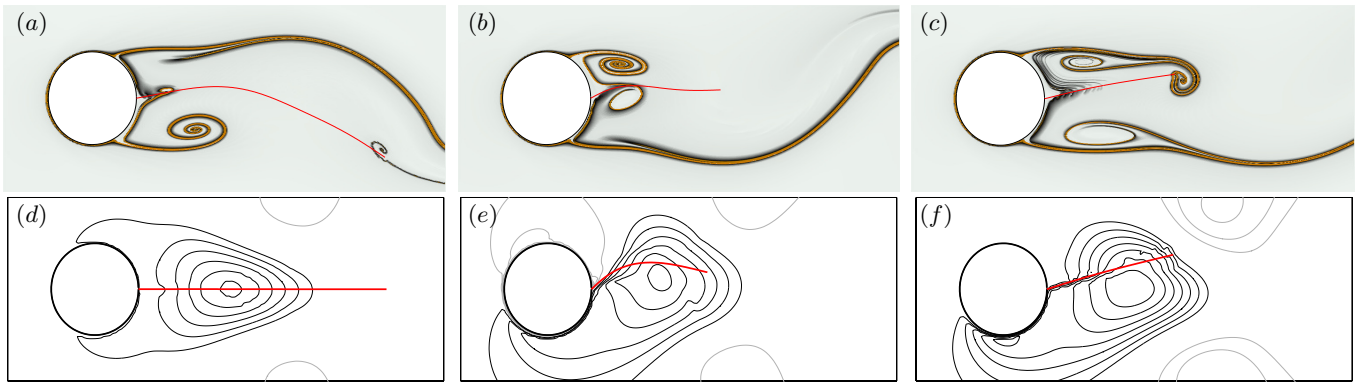

FIG. 4: Left, center and right columns correspond, respectively, to long/flexible (case ①), short/flexible (case ②) and short/stiff filaments (case ③). Top row shows instantaneous snapshots of maximum value of FTLE and filament position (red line). Bottom row shows mean filament position (red line) and mean pressure distortion. The latter is defined as the difference between the time-averaged pressure field with and without the filament. Positive (negative) distortions are plotted with solid black (gray) contour lines; positive pressure distortion in the lee side of the cylinder signals reduced pressure drag, while asymmetric distortion with respect to the x-axis indicate that a net y-force is generated. The pressure field is averaged across neighboring grid cells around the fluid-solid interface to eliminate small numerical oscillations linked to the immersed-boundary approximations. Supplementary online movies are available.

pressure distribution in the near cylinder wake (Fig. 4(d-f)).

The vorticity induced by the short filaments does not only result in a non-zero mean lift force and torque because of broken symmetry, but also in a reduced mean drag force. Significantly, cf. table I, asymmetric flapping always result in a smaller *total* mean drag (i.e. including the drag force on the filament) than for a cylinder alone. A similar drag-reducing mechanism has been observed [19–21] when a number of short filaments ($L \approx 1/4$) is distributed over the rear side of a cylinder. In this context, it is interesting to mention recent observations [22, 23] that the von Kárman vortex shedding can be significantly altered in the range $47 < Re < 100$ by placing a second small object approximately at a 45 degree angle from the $y = 0$ axis and around $1 - 2$ diameters downstream of the cylinder. In fact, it was found that the vortex shedding can be stabilized altogether up to $Re = 70$. Our results show that the filament tethered at the rear end of the cylinder, oscillates in the proximity of the most sensitive regions identified in [23], with an ensuing favorable effect on the wake dynamics.

	L	R_2	C_d	C_l	C_q	f_c
C	0.0	—	1.36 ± 0.01	0.00 ± 0.34	0.00	0.164
①	3.0	0.005	1.28 ± 0.06	0.00 ± 0.23	0.00	0.157
②	1.5	0.005	1.32 ± 0.08	0.18 ± 0.28	0.01	0.159
③	1.5	0.100	1.23 ± 0.05	0.21 ± 0.24	0.02	0.145

TABLE I: Total mean drag, lift, torque coefficients (C_d, C_l, C_q, respectively) and Strouhal number (f_c) at $Re = 100$ in the absence of a filament (C) and for three different filaments (cases ①-③). Values after the $\pm$ sign denote the oscillation amplitudes around the means. C_d and C_l are normalized with $1/2\,\rho_f\,U^2\,D$, whereas C_q is normalized with $1/2\,\rho_f\,U^2\,D^2$.

We have shown that the presence of passive short filaments in unsteady wakes can generate lift without increasing drag. Such filaments may thus in many circumstances favor the hydro- or aero-dynamic behavior of bluff body wakes. Numerous observations [24] suggest that animals control the flow around their bodies in order to reduce drag by making use of their pelage, of scales, feathers and other appendages, with a wide range of textures, rigidities, lengths, and active under different Reynolds numbers. In many cases the functional role of appendages is not fully understood, as their complex motion varies greatly depending on the task being carried out. The pteropod *Clione antarctica* is one example: equipped with three bands of cilia as well as a pair of wings, it possesses two distinct modes of swimming: ciliary mode and flapping mode. While flapping, significant – possibly passive – movement of the cilia is observed but the functional role of this movement is not yet clear [25]. Based on the results presented here it can be speculated that even passive, apparently inert cilia have a positive influence on the locomotion of flying and swimming animals.

We thank J. Pralits, D. Natali and A. Pinelli for fruitful discussions. The first author acknowledges financial support from the European Commission for Research (FP7-PEOPLE-2010-IEF-272335-REDWING).

[1] R.D. Averitt, Nature Physics **6**, 639 (2010)
[2] J.D. Crawford and E. Knobloch, Annu. Rev. Fluid Mech. **23**, 341 (1991)
[3] N. Vandenberghe, J. Zhang and S. Childress, J. Fluid Mech. **506**, 147 (2004)
[4] S. Alben ans M.J. Shelley Proc. Natl. Acad. Sci. U.S.A. **102**, 11163 (2005)
[5] H. Gadelha, E.A. Gaffney, D.J. Smith and J.C. Kirkman-Brown, J. Roy. Soc. Interface **7**, 1689 (2010)
[6] H. Kellay, X-l. Wu and W.I. Goldburg Phys. Rev. Lett **74**, 3975 (1995).
[7] J. Zhang, S. Childress, A. Libchaber and M. Shelley, Nature **408**, 835 (2000)
[8] L. Zhu and C.S. Peskin, J. Comp. Phys. **179**, 452 (2002)
[9] M.J. Shelley and J. Zhang Annu. Rev. Fluid Mech. **43**, 449 (2011)
[10] C.S. Peskin, Acta Numerica **11**, 479 (2002)
[11] Y. Kim and C.S. Peskin, Phys. Fluids **19**, 053103 (2007)
[12] K. Taira and T. Colonius, J. Comp. Phys. **225**, 2118 (2007)
[13] B. J. Connell and D.K.P. Yue, J. Fluid Mech. **581**, 33 (2007)
[14] M. Argentina and L. Mahadevan Proc. Natl. Acad. Sci. U.S.A. **102**, 1829 (2005)
[15] M.S. Triantafyllou and C.T. Howell, J. Sound Vib. **173**, 433 (1994)
[16] L.E. Becker and M. Shelley, Phys. Rev. Lett. **87**, 198301 (2001)
[17] G. Haller, Phys. Fluids **13**, 3365 (2001)
[18] G. Boffetta, G. Lacorata, G. Redaelli and A. Vulpiani, Physica D **159**, 58 (2001)
[19] J. Favier, A. Dauptain, D. Basso and A. Bottaro, J. Fluid Mech. **627**, 451 (2009)
[20] J. Niu and D.L. Hu, Phys. Fluids **23**, 101701 (2011)
[21] S. Kunze and C. Brucker, C.R. Mécanique, **340**, 41 (2012)
[22] P.J. Strykowski and K.R. Sreenivasan, J. Fluid Mech. **218**, 71 (1990)
[23] F. Giannetti and P. Luchini, J. Fluid Mech. **581**, 167 (2007)
[24] F.E. Fish and G.V. Lauder, Annu. Rev. Fluid Mech. **8**, 193 (2006)
[25] S. Childress and R. Dudley, J. Fluid Mech. **498**, 257 (2004)
[26] We discretize the fluid equations with a staggered-grid, finite-volume formulation using second order semi-implicit time integration. The no-slip boundary condition is enforced at Lagrangian points by appropriate regularized surface forces [10–12]. A grid size of $h = 1/60$ is sufficient to reproduce previous work [12, 13] for the flow past a cylinder – in terms of lift/drag coefficients for various Re – and for the 2D "flag" problem – in terms of straight/flapping motion for various R_1 and R_2.
[27] See supplementary material at *http://www.mech.kth.se/∼shervin/filament/* for movies of the three filaments.